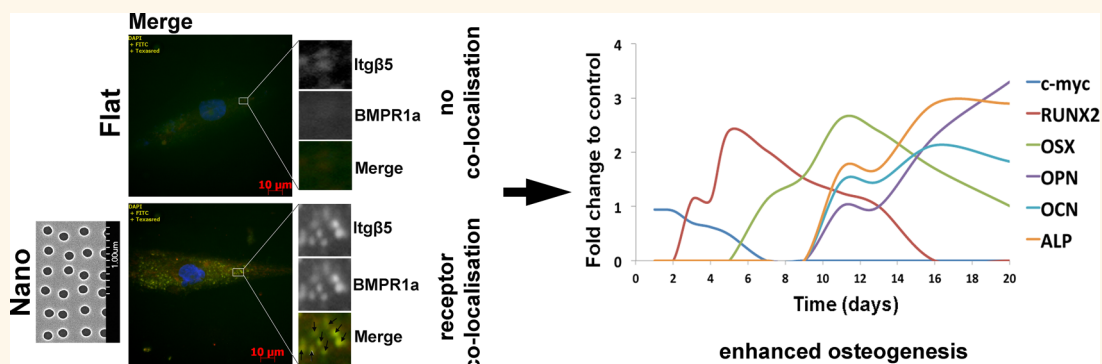


Nanotopographical Induction of Osteogenesis through Adhesion, Bone Morphogenic Protein Cosignaling, and Regulation of MicroRNAs

Jingli Yang,[†] Laura E. McNamara,[†] Nikolaj Gadegaard,[§] Enateri V. Alakpa,[†] Karl V. Burgess,[‡] R. M. Dominic Meek,[‡] and Matthew J. Dalby^{*†}

[†]Centre for Cell Engineering, Institute of Molecular, Cell and Systems Biology, College of Medical, Veterinary and Life Sciences, Joseph Black Building, University of Glasgow, Glasgow, G12 8QQ, U.K., [‡]Scottish Polyomics Facility, Wolfson Wohl Cancer Research Centre, College of Medical, Veterinary & Life Sciences, University of Glasgow, Garscube Estate, Glasgow G61 1QH, U.K., [§]Division of Biomedical Engineering, School of Engineering, University of Glasgow, Glasgow, G12 8LT, U.K., and [‡]Department of Orthopaedics, Southern General Hospital, 1345 Govan Road, Glasgow G514TF, U.K.

ABSTRACT



It is emerging that nanotopographical information can be used to induce osteogenesis from mesenchymal stromal cells from the bone marrow, and it is hoped that this nanoscale bioactivity can be utilized to engineer next generation implants. However, the osteogenic mechanism of surfaces is currently poorly understood. In this report, we investigate mechanism and implicate bone morphogenic protein (BMP) in up-regulation of RUNX2 and show that RUNX2 and its regulatory miRNAs are BMP sensitive. Our data demonstrate that osteogenic nanotopography promotes colocalization of integrins and BMP2 receptors in order to enhance osteogenic activity and that vitronectin is important in this interface. This provides insight that topographical regulation of adhesion can have effects on signaling cascades outside of cytoskeletal signaling and that adhesions can have roles in augmenting BMP signaling.

KEYWORDS: nanotopography · mesenchymal stem cells · metabolomics · osteogenesis · BMP and integrin signaling

Adherent cells perceive extrinsic signals by sensing the composite features (biochemical and/or biophysical) of the extracellular matrix (ECM). In turn, these signals govern a plethora of cellular responses, including migration, proliferation, differentiation and gene expression.^{1–8} Biophysical features of the ECM can be on the nanoscale, and this has driven the development of nanoscale biomaterials to help understand the potential of nanotopography in

modulating cell responses to suit particular research and therapeutic applications. Over the past decade, many reports have illustrated changes in the behavior of cells to nanoscale substrates in a wide range of cells, including human endothelia,⁹ osteoblasts,¹⁰ fibroblasts,¹¹ muscle cells,¹² mesenchymal stem cells,^{8,13–17} and even embryonic stem cells.^{18–21}

For bone regeneration, bone marrow derived human mesenchymal stromal cells

* Address correspondence to matthew.dalby@glasgow.ac.uk.

Received for review March 11, 2014 and accepted September 16, 2014.

Published online September 16, 2014
10.1021/nn504767g

© 2014 American Chemical Society

(hMSCs) hold great promise as an autologous cell source that can differentiate into mature osteoblasts.^{22,23} These are the adherent population of the bone marrow and include osteoprogenitors and multipotent skeletal stem cells.^{24,25}

A range of studies have focused on nanotopographical induction of bone formation (osteoinduction). The rules for topographical guidance of cells, including hMSCs, are perhaps not as straightforward as for stiffness, where physiological stiffnesses define hMSC fate,^{26–28} and substrate chemistry, where tissue specific chemistries can induce desired phenotypes.^{29,30} Rules, however, are slowly emerging,³¹ and there are a rapidly growing number of studies in this area. For example, studies have shown hMSC osteogenesis arising from culture on TiO₂ nanotubes. One study showed that hMSCs osteogenic differentiation was best achieved with a tube diameter of 100 nm,³² while another study indicated, using rat-derived MSCs, that optimal osteogenic differentiation was achieved with smaller diameters down to 15 nm.^{33,34} Sub-20 nm high topographical features^{35,36} and nanohelices with collagen-like 67 nm banding¹⁶ have also been shown to be osteogenic.

One of the best described osteogenic nanotopographies has been fabricated by electron beam lithography.³⁷ The surface, near-square 50 (NSQ50), has an offset of up to ± 50 nm from a perfect square lattice arrangement of 120 nm diameter, 100 nm deep pits with 300 nm center–center spacing and can specifically promote hMSCs to differentiate into osteoblasts with similar efficiency to osteogenic medium.⁸ This partial disorder, but not total randomness, is important because if the offset is zero, the retention of multipotency results in the maintenance of a stem cell population, rather than the induction of differentiation.¹³ The surface has similarities to the morphology of collagen X, a nonfibrillar collagen found during endochondral ossification and nonunion fracture repair that has a nanoscale disordered (but not random) hexagonal arrangement.³⁸ The surface has further advantages as the fabrication process means that exact replicates can be manufactured and, through use of nickel shims, many replicas injection molded into plastics with high fidelity. It is facile in that it has been shown to exert osteogenic effect when embossed or injection molded into a range of biocompatible polymers.^{39–41} These features make the surface an ideal candidate for further study of nanotopographical control of osteogenesis.

To date, efforts to understand the process by which cells interpret nanotopographical cues have been focused on focal adhesion interactions and the resulting changes in intracellular tension. It has been proposed that nanotopography can modulate integrin clustering and focal adhesion formation, and in turn regulate stem cell function and differentiation.^{13,14,42–44}

Such alterations may result in the modulation of interfacial forces to guide cytoskeletal organization and the organization of transmembrane receptors, and thus may subsequently regulate the intrinsic signaling of the cells.⁴⁵ This may occur through, for example, focal adhesion kinase (FAK) and G-proteins,^{42,46} feeding into major signaling cascades such as the mitogen activated protein kinase-extracellular signal regulated kinase (MAPK-ERK) 1/2 pathway, and c-jun n-terminal kinase (JNK) pathway.^{14,47}

However, other key pathways have been less well studied, if at all, in relation to nanotopography-driven osteogenesis. Bone morphogenetic proteins (BMPs), especially BMP2, play a pivotal role in adult skeletal development and bone formation, and *in vivo* studies have demonstrated that BMP receptor signaling is essential for normal bone formation.⁴⁸ BMP signals activate the osteogenic transcription factors RUNX2 (runt-related transcription factor 2) and/or osterix, mediated by SMAD proteins, to modulate bone matrix protein expression (canonical BMP signaling).^{49–51} BMPs may also function through p38MAPK and JNK cascades, (noncanonical BMP signaling) similar to those characterized for integrin signaling pathways.⁵² A recent study of human osteoblastic differentiation showed that the BMP2 signal exerts its function by cooperation with the integrin α/β pairing. The authors demonstrated that the BMP2 and integrin receptors could colocalize, and that this synergistic pairing enhanced BMP2 signaling and osteogenesis.⁵³

In this study, we examine the temporal expression of osteogenic genes by hMSCs/progenitors induced by the NSQ5050 nanotopography and relate findings to classical Stein and Lian timelines,⁵⁴ to indicate normal osteogenic progression on the NSQ5050 nanotopography. We update these timelines with information on transcriptional control, RUNX2 and osterix (OSX), and investigate very early commitment events. For the first time, to our knowledge, we show that BMP and BMPR1a are up-regulated ahead of RUNX2 and that RUNX2 and its regulatory miRNAs are BMP sensitive, that the nanofeatures promote colocalization of integrins and BMP2 receptors in order to enhance osteogenic activity and that vitronectin is important in this interface.

RESULTS AND DISCUSSION

Temporal Gene Expression Patterns. For osteogenesis to occur a sequence of genes needs to be activated in the correct order to permit proliferation and differentiation. Three principal development periods (proliferation, ECM maturation and mineralization) have been defined by the sequential expression of the genes associated with each phase.⁵⁴ In this progression cell cycle and growth genes (*i.e.*, *c-fos* and/or *c-myc*) are downregulated to end proliferation and this is followed by the process of differentiation, with expression of genes

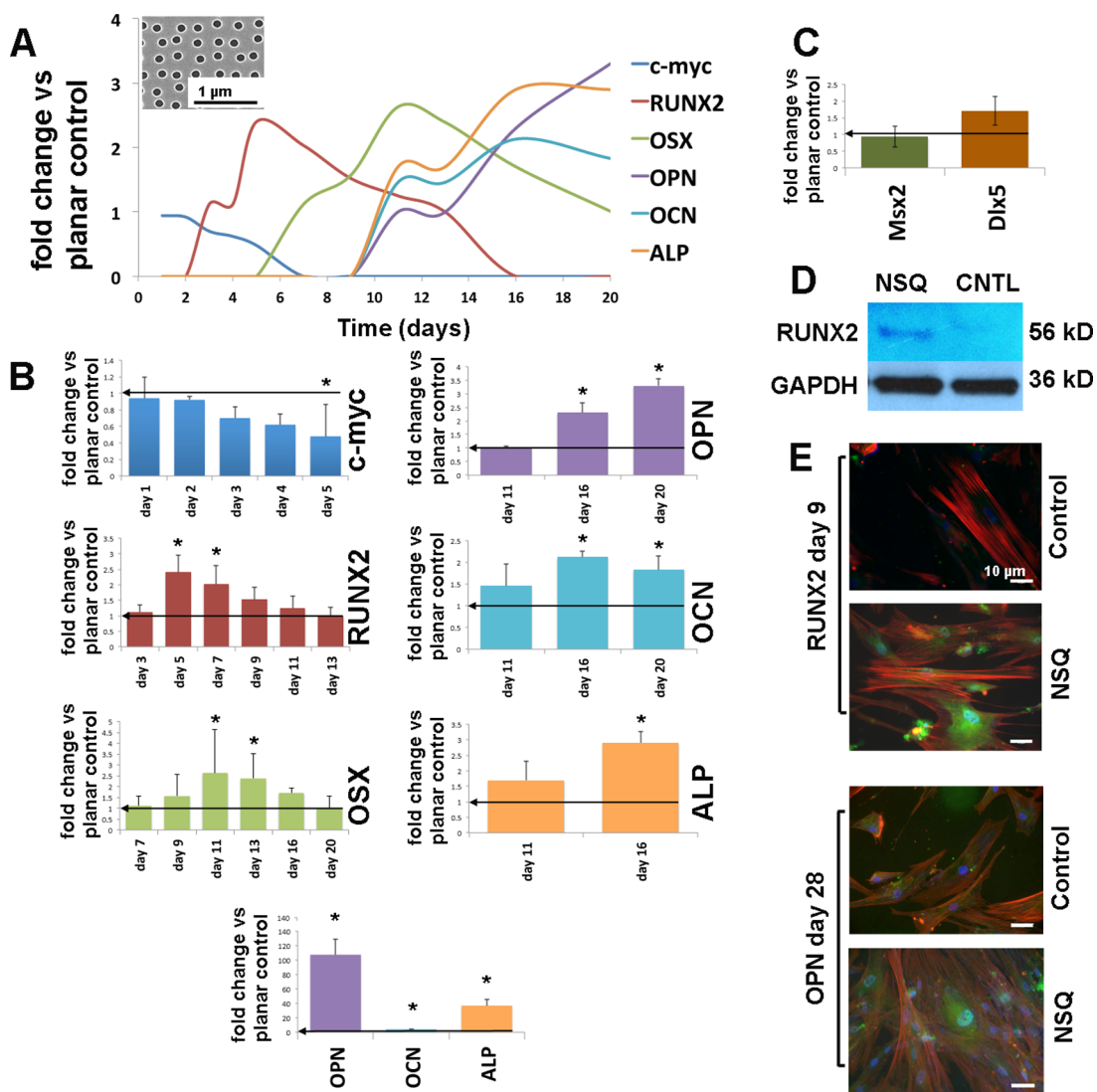


Figure 1. Temporal analysis of osteogenic phenotypical expression on the nanotopography NSQ50 (NSQ, A inset) with all data relative to MSCs cultured on planar control. (A) Line plot showing expression of proliferative, transcriptional and extracellular matrix related genes involved in osteogenesis assessed by qPCR. The data shows a slow increase in proliferation and increase in transcriptional control (RUNX2 and then OSX) by days 5–11 followed by increasing expression of bone matrix related genes (OCN, OPN and ALP) in MSCs on NSQ50 compared to on planar control. (B) Individual histograms showing the data used to make the line plot (the plot in A is only made from the data in these histograms, joined points are best fit where data is missing) also show day 28 data for OPN, OCN and ALP, as expression was too high to use on the line plot. (C) Gene expression of Msx2 and Dlx5 by qPCR showing no change relative to control and indicating RUNX2 related OSX activation. (D) Western blot of RUNX2 at 5 days of culture confirming qPCR data at the protein level (CNTL = planar control). (E) Immunofluorescence of RUNX2 (9 days) and OPN (28 days) showing increased expression on NSQ50 compared to control and confirming qPCR data. For fluorescence microscopy red = actin, blue = nucleus and green = RUNX2 or OPN. For qPCR data = mean \pm SD for $n = 3$ independent experiments (3 material replicated per experiment), *ANOVA $p < 0.05$. Arrows on graphs show the control level. CNTL = planar control, NSQ = NSQ50.

encoding ECM proteins that prepare the matrix for mineralization. Hence, to study growth, transcriptional control and ECM maturation for cells cultured on NSQ50 nanotopography, the growth modulator c-myc, the transcription factors RUNX2 and OSX and the extracellular maturation proteins alkaline phosphatase (ALP), osteopontin (OPN) and osteocalcin (OCN) were examined at the transcript level over a 28 day timecourse for osteoprogenitors cultured on NSQ50 embossed into polycaprolactone (PCL) (Figure 1A,B) using quantitative (q-RT) PCR. All data is presented relative to control cells on planar PCL surfaces (Figure 1B,C).

By day 5, c-myc was down-regulated on NSQ50 compared to cells cultured on the planar control. Following the repression of growth-related signaling, transcripts related to osteogenic control were up-regulated. After 5 days of culture, while c-myc was becoming repressed, the expression of RUNX2 had significantly increased on NSQ50. RUNX2 was maximally expressed at the day 5 time-point, which was followed by a peak in OSX expression at day 11 compared to baseline expression in cells on control. Up-regulation of RUNX2 in conjunction with the repression of c-myc expression has been reported

elsewhere,^{55,56} which is sensible as differentiation occurs in hand with decreased cell growth. RUNX2 plays a central role in the regulation of bone matrix proteins,^{57,58} and OSX is a zinc finger transcription factor that controls downstream pathways in bone formation that are either dependent on, or independent of, RUNX2.^{59,60} RUNX2-independent initiation of OSX is mediated by either Msx2 or Dlx5. To examine the levels of Msx2 and Dlx5 immediately prior to the OSX peak, we examined expression levels at day 9. No significant change in expression levels of Msx2 and Dlx5 were noted compared to cells on planar control and thus, we propose that the NSQ50 surface induced OSX expression in a RUNX2-mediated manner (Figure 1C). It is important that after a brief increase in RUNX2 expression on NSQ50 that it is subsequently down-regulated, as prolonged expression can lead to slower bone growth,⁶¹ and even enhance bone resorption.⁶²

ALP, which is involved in producing free phosphate for use in mineralization, was then highly expressed at day 16–28, concomitant with increased expression of OCN, which is a key marker of bony differentiation involved in the sequestration of calcium for mineralization. It is interesting that very high levels of OPN were noted, especially by day 28, in excess of the levels of OCN (Figure 1B). This is slightly at odds with classical osteogenic timelines that indicate that both OCN and OPN should be highly expressed at this time-point.⁵⁴ However, it is perhaps logical that progenitors being osteoinduced by material interactions would use OPN, as it contains the adhesive tripeptide motif RGD (arginine, glycine, aspartic acid), whereas OCN does not. Furthermore, MSCs are known to form super-mature adhesions (adhesions >5 μm long) on the NSQ50 surface, to support increased intracellular tension and the endogenous expression of RGD-containing proteins would facilitate the assembly of large adhesions. RUNX2 and OPN expression was confirmed at the protein level using Western blotting (Figure 1D) and immunofluorescence (Figure 1E).

Temporal Metabolite Signaling. Employment of untargeted metabolomics at very early time points (days 3, 5 and 7) was used to try and direct subsequent experiments on mechanism (*i.e.*, use of an untargeted approach to provide targets) and provided some interesting trends. Metabolites linked to MAPK signaling were down-regulated with time suggesting a reduction in proliferative signaling⁶³ and reflecting the c-myc mRNA data (Figure 2). However, metabolites that have been linked to calcium signaling tended to be up-regulated, particularly at day 5 (Figure 2). This is interesting as calcium signaling has been linked to BMP2 signaling⁶⁴ and this provides rational for study of BMP2 as an early stage event in materials induced osteogenesis. Other notable metabolites were likely involved in amino acid metabolism (up and down-regulations),

growth (down-regulated) and energy (becomes down-regulated) (Figure 2). While only a small number of metabolites were identified that were involved at all time points, the analysis highlights interactions with proliferation and differentiation control tying in well with results discussed in Figure 1. Kyoto Encyclopedia of Genes and Genomes (KEGG) analysis revealed changes in fatty acid biosynthesis pathways suggesting alterations in energy demand in MSCs on NSQ50 compared to control (Supporting Information, Figures S1–S3). It is noted that changes were quite small, but it is likely that the cells were in a lag phase in this early stage of culture on the nanotopography.

BMP2 Switches on RUNX2. It would be expected that a reduction in cell proliferation and activation of RUNX2 would be controlled by extrinsic factors to initiate osteogenesis. Thus, with help of the above data from temporal metabolomic analysis (Figure 2), we investigated the role of bone morphogenic protein 2 (BMP2)⁶⁵ in the activation of RUNX2 on the NSQ50 nanotopography. QPCR comparison of cells on NSQ50 compared to planar control at days 1–11 showed that by day 3 the BMP2 receptor, BMPR1a, was significantly up-regulated and by day 5, BMP2 itself and RUNX2 were also up-regulated (Figure 3A). This suggests that the cells were primed for BMP signaling ahead of RUNX2 activation. Of course, cell culture media contains many proteins including, *e.g.*, transforming growth factor (TGF) β (BMP belongs to the TGF superfamily).⁶⁶ Hence, we used low serum media (containing 1% serum; the MSCs were dead within 48 h with 0% serum) to see if RUNX2 expression still occurred. Immunofluorescence indicated localization of RUNX2 within the nucleus even in low serum, and this indicates that the cells were producing endogenous BMP2 in response to the NSQ50 surface (Figure 3A inset).

We reaffirmed up-regulation of BMP2 and its receptor, BMPR1a at the transcript level showing they were significantly up-regulated at day 3 in cells on NSQ50 compared to control (Figure 3B) and then used qPCR to demonstrate that the downstream intracellular signaling molecules SMAD1 and SMAD5 were highly expressed relative to controls at day 5 (Figure 3C). The engagement of BMP2 with its receptor, BMPR1a, phosphorylates SMAD messengers, and the phosphorylated SMADs then translocate into the nucleus and are recruited by RUNX2 to initiate transcription from BMP-responsive genes.⁴⁹

To investigate the relation of the BMP2 signal to the induction of transcription from the RUNX2 gene, progenitors cultured on the NSQ50 topography and planar control were treated with the BMP2 antagonist noggin for 5 days. RUNX2 expression was measured by qPCR and Western blotting to determine the transcript and protein-level responses. If the BMP signal was blocked, RUNX2 was inhibited back to control levels, indicating that RUNX2 expression was BMP-dependent

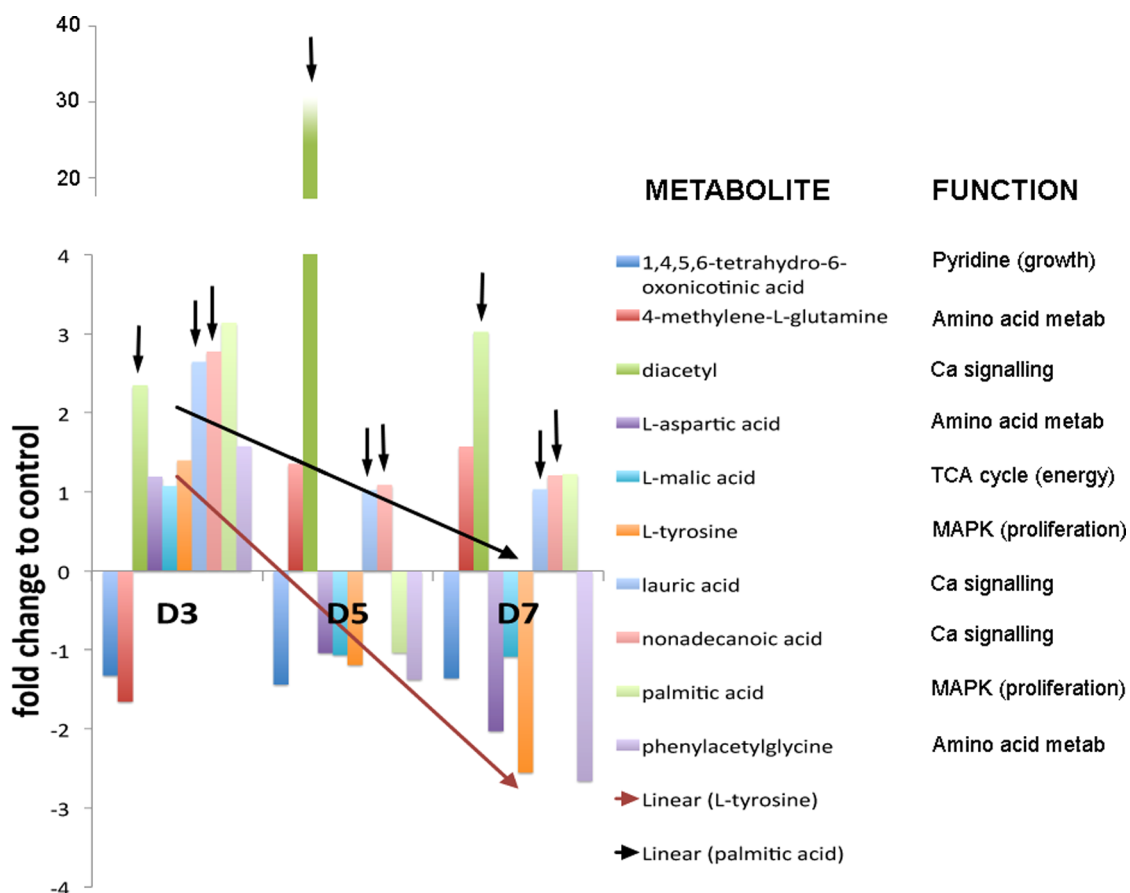


Figure 2. Temporal metabolite analysis for metabolites extracted from MSCs cultured on NSQ50 compared to MSCs cultured on planar control. Eleven metabolites were identified at all time-points (days 3, 5 and 7) with roles in proliferation (MAPK), growth, amino acid metabolism, Ca^{2+} signaling and energy (functions identified via the Ingenuity Pathway database). The trends for MAPK-related metabolites was that of down-regulation with time (trend-line arrows: red and black linear), the trend for Ca^{2+} signaling-related metabolites was general up-regulation (vertical arrows). Graph shows mean of $n = 3$ material replicates at each time point. Note that L-tyrosine and L-aspartic acid were identified by use of standards and the others were annotated by mass and retention time (see Materials and Methods).

(Figure 3D; densitometry of the band provides arbitrary values of 35.5 for NSQ and 27.9 for NSQ with noggin). Furthermore, if progenitors were cultured for up to 28 days on NSQ50 with noggin, OPN production was reduced back to control levels (Figure 3E), indicating that the osteogenesis was regulated by BMP2 via RUNX2.

We note that the activation of BMPs can also trigger SMAD-independent signaling pathways, including ERK, mitogen-activated protein kinase p38 (p38MAPK) and JNK, which have previously been implicated in materials-driven osteogenesis through integrin dependent pathways.^{14,47,52} For these pathways to be activated by BMP2 in a SMAD-independent manner, interaction of bone morphogenetic protein receptor associated molecule 1 (BRAM1) or X-linked inhibitor of apoptosis protein (XIAP), and downstream TGF β activated kinase 1 (TAK1) and activation of its binding protein (TAB1) activation have to be initiated.⁶⁶ There was no statistically significant difference observed in Tab1 gene expression between cells on NSQ50 substrates and on the planar control (Figure 3F). This suggests that

NSQ50-initiated osteogenesis is not reliant on SMAD-independent BMP signaling.

BMP2 Receptor Colocalizes with Integrins. To further investigate the mechanisms of NSQ50 osteogenic differentiation, we examined the expression of integrin subunits $\alpha 3$, $\alpha 4$, αv , $\beta 1$, $\beta 3$ and $\beta 5$. Significant up-regulation of integrin subunits $\alpha 4$, αv and $\beta 5$ relative to planar controls were noted at day 5 (Figure 4A). Integrins are the receptors that primarily link adherent cells to the ECM and these receptors play an indispensable role in cell adhesion, migration, proliferation and differentiation in many cell types.⁶⁷ Integrin binding with ECM components depends upon the pairing of α and β units, and it is widely accepted that the pairing of αv with $\beta 1/\beta 3/\beta 5$ and $\alpha 5$ with $\beta 1$ binds to the RGD motif in OPN, and fibronectin (mainly $\alpha v\beta 3$) and vitronectin (primarily $\alpha v\beta 5$ but also can use $\alpha v\beta 3$) in ECM.⁶⁷ As integrin $\beta 5$ had been highlighted by our analysis, suggesting a key role for vitronectin in adhesion to the nanopatterned surface, we blocked this subunit using an antagonistic antibody, and observed the effect on RUNX2 expression. However, the data

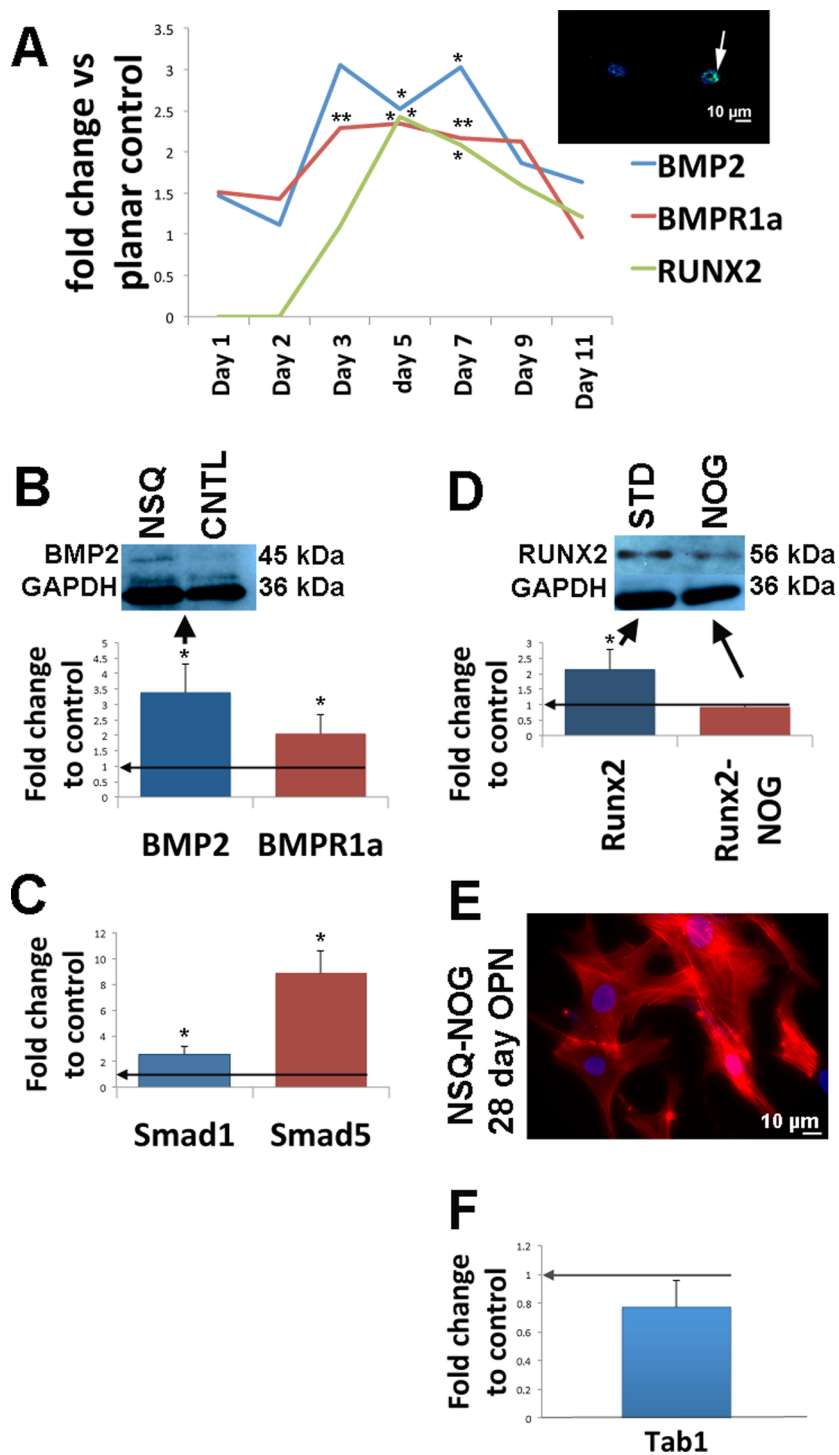


Figure 3. BMP2 analysis of nanotopography stimulated osteogenic phenotypical expression. (A) Temporal profile of BMP2 and its receptor BMPR1a compared to RUNX2 for MSCs cultured on NSQ50 compared to control showing that BMP and BMPR1a are up-regulated ahead of RUNX2 and are maintained through RUNX2 expression (inset RUNX2 localization within the nuclei of MSCs cultured on NSQ50 in low serum media). (B) Gene up-regulation of BMP2 and its receptor BMPR1a were assessed by qPCR and the up-regulation of BMP2 was confirmed using Western blotting after MSCs were cultured on the NSQ50 surface for 3 days compared to on planar controls. (C) The abundance of BMP signal intracellular signaling molecules SMAD1 and SMAD5 was also increased at 3 days cell culture on NSQ50 compared to planar control. (D) The inhibition of the BMP2 signal by noggin resulted in a return to control levels of the osetogenic transcription factor RUNX2 at both gene and protein level after MSCs were cultured on NSQ50 for 5 days compared to on planar control. (E) With longer culture (28 days) MSCs on the NSQ surface did not express osteopontin. (F) Gene expression of Tab1 by qPCR in MSCs cultured on NSQ50 surface showed no difference to on planar control. This data shows that RUNX2 and subsequent osteoblast phenotype development on NSQ50 is BMP and SMAD dependent. For fluorescence microscopy red = actin, blue = nucleus and green = OPN. For qPCR data = mean \pm SD for $n = 3$ independent experiments (3 material replicates per experiment), *ANOVA $p < 0.05$. Arrows on graphs show the control level. CNTL = planar control, NSQ = NSQ50, NOG = noggin, STD = standard culture media.

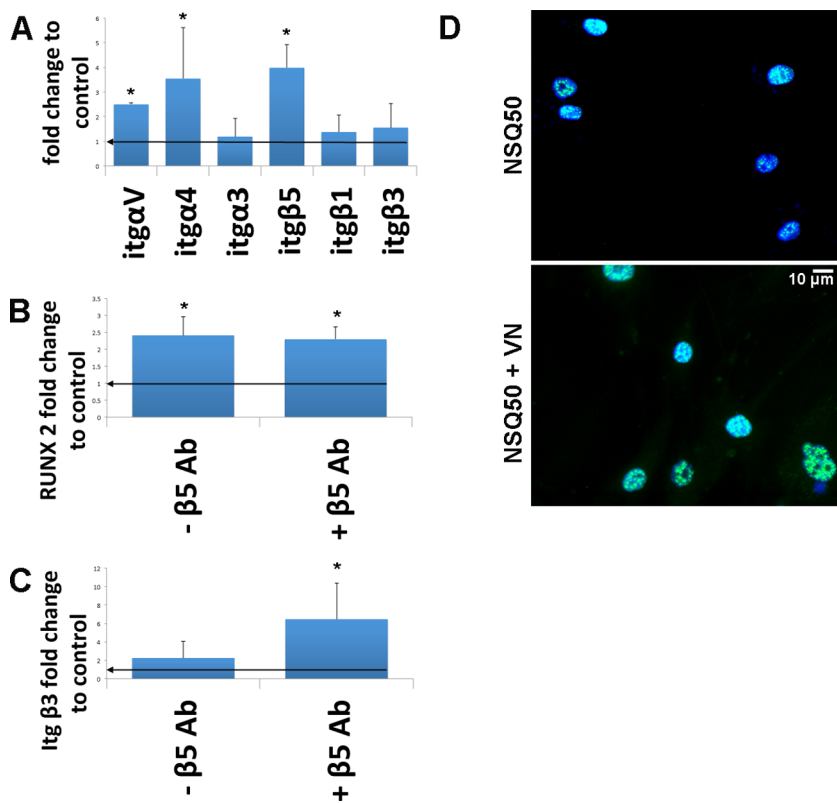


Figure 4. Integrin expression in response to NSQ50 nanotopography. (A) Integrins α V, α 4 and β 5 were up-regulated at the gene level after 5 days culture on NSQ50, and it is notable the α V β 5 makeup the vitronectin receptor. (B) However, inhibition of β 5 with antibodies ($-\beta$ 5 Ab = standard culture, $+\beta$ 5 Ab = inhibition) did not alter expression of the osteogenic transcription factor RUNX2. (C) Concomitantly with inhibition of β 5, the other possible vitronectin β subunit, β 3, became up-regulated. (D) Immunofluorescent staining of RUNX2 in MSCs cultured on NSQ50 or NSQ50 precoated with vitronectin (VN) showing increased RUNX2 expression with coated surfaces (blue = DAPI, green = RUNX2). Together, the results illustrate a likely role for the vitronectin receptor in topographically driven osteogenesis. For qPCR data = mean \pm SD for $n = 3$ independent experiments (3 material replicated per experiment), *ANOVA $p < 0.05$. Arrows on graphs show the control level.

suggested that integrin β 5 was not directly linked with the up-regulation of RUNX2, since the abundance of RUNX2 transcripts on NSQ50 were not significantly different with or without β 5 blocked (Figure 4B). However, looking at β 3 expression when β 5 was blocked showed that this other subunit that cells can also exploit to bind to vitronectin becomes up-regulated suggesting cellular redundancy and that the cells could still exploit vitronectin even with β 5 unavailable (Figure 4C) despite β 3 not being up-regulated by standard culture of MSCs on NSQ50 (Figure 4A). To test the role of vitronectin further, we cultured MSCs on NSQ50 coated with vitronectin (uncoated NSQ50 acting as control) and stained for RUNX2 after 5 days of culture. While all cells were RUNX2 positive, with RUNX2 localized to the cell nuclei on the standard NSQ50 surfaces, RUNX2 expression was notably more intense when cultured on NSQ50 precoated with vitronectin (Figure 4D).

To study the vitronectin receptor further, we considered recent studies that showed integrins could exert their effects on cells through crosstalk with other ECM components, such as TGFs,^{68,69} including BMP2.⁵³ Therefore, we proposed that there was a functional relation between these two signals. Double

immunostaining using specific β 5 and BMPR1 antibodies demonstrated the colocalization of these two receptors in hMSCs on the NSQ50 surface (Figure 5A). However, on the planar surface, while β 5 could be seen as part of the adhesion, no colocalization was noted (Figure 5A). This observation was confirmed in the whole cell population by coimmunoprecipitation (Figure 5B; we note that only very small protein yields were obtained after lysis and pull-down from the material surfaces). Furthermore, when the BMP2 signal was blocked using noggin, up-regulation of integrins α V, β 4 and β 5 (as identified in Figure 4) were abrogated back to planar control levels, accompanying the down-regulation of the osteoblastic phenotype (Figure 5C). This suggests that BMP2 might help mediate integrin-related signaling in response to the osteogenic nanotopography. It could be postulated that this may help with the formation of supermature adhesions (adhesions $>5 \mu\text{m}$ in length) that have been shown to be necessary to support the high levels of intracellular tension required by the cells during the osteogenesis of hMSCs.^{14,47,70–72} It could be further speculated that use of vitronectin receptors is important in osteogenesis as the cells need to form the super mature

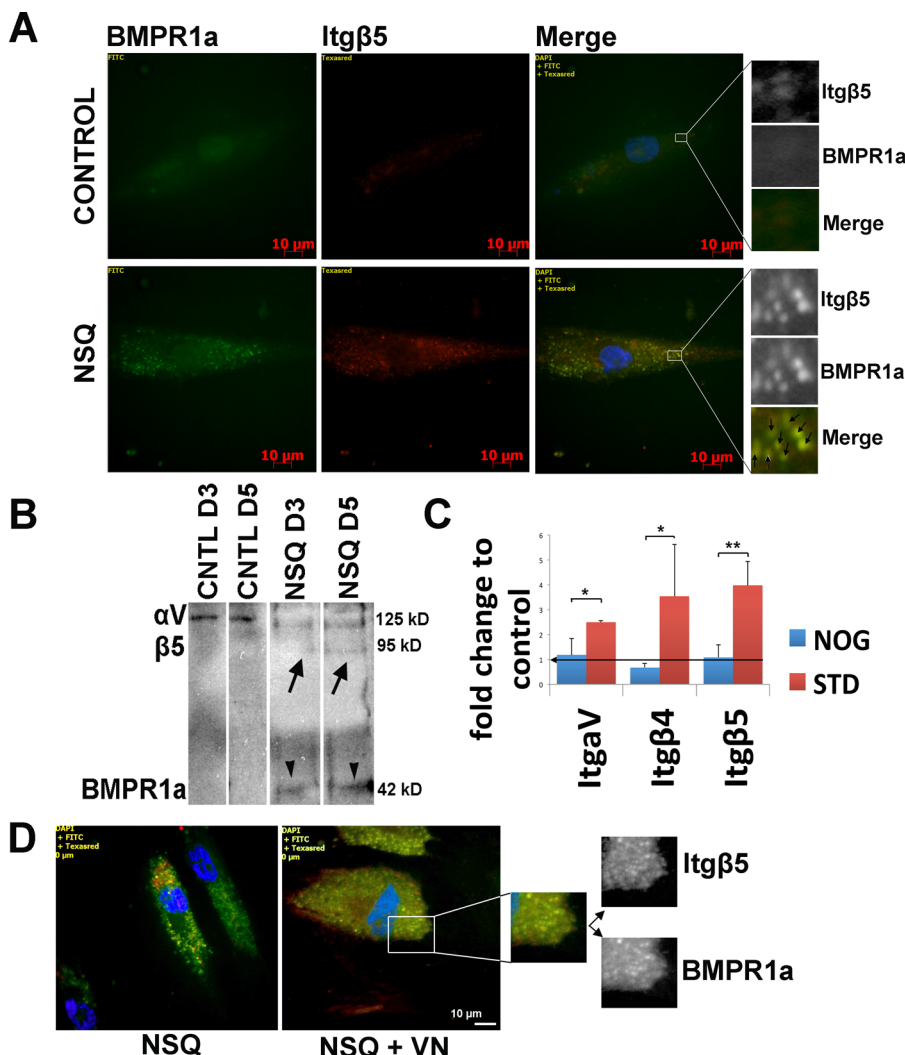


Figure 5. Integrins colocalize with the BMP2 receptor when cultured on NSQ50. (A) Double immunostaining after 5 days cell culture of MSCs on the NSQ50 surface and planar control using integrin β 5 (red) and BMPR1a (green) specific antibodies. Only MSCs cultured on NSQ50 demonstrated colocalization (yellow and arrows in the outset merge). On planar control, while integrin expression in adhesions was seen (outset Itg β 5), colocalization to BMPR1a was not. (B) The colocalization of integrin β 5 and BMPR1a was confirmed by coimmunoprecipitation using $\alpha v\beta 5$ (arrows) and BMPR1a (arrowheads) specific antibodies. (C) Gene expression of integrins was assessed by qPCR after the BMP signal was inhibited by noggin. Integrins (αv , $\beta 4$, and $\beta 5$) were down-regulated compared to MSCs without noggin treatment. (D) Colocalization (yellow) of Itg β 5 (red) and BMPR1a (green) was increased for NSQ50 precoated with vitronectin (VN) compared to uncoated NSQ50 surfaces with dense receptor copositioning seen (outset). For qPCR data = mean \pm SD for $n = 3$ independent experiments (3 material replicated per experiment), *ANOVA $p < 0.05$, ** $p < 0.01$. Arrow on graph shows the control level. For immunofluorescence, blue = DNA. NSQ = NSQ50, NOG = noggin.

adhesions and use of vitronectin allows the cells to bridge from one set of integrins to the next as a part of a single, larger, adhesion than, e.g., fibronectin.⁷³

The potential role of vitronectin was further investigated by repeating the dual Itg β 5/BMPR1a staining but on NSQ50 precoated with vitronectin. Figure 5D shows increased colocalization of the receptors in MSCs cultured on vitronectin coated NSQ50 compared to standard NSQ50 surfaces. This indicates that vitronectin helps mediate the nanotopographically induced receptor colocalization.

BMP2 and Nontranscriptional Regulation. MicroRNAs are classified as noncoding regulatory RNAs acting in diverse biological processes, predominantly by mediating

the translational repression of their target mRNA species. Recent studies have shown miRNAs play important roles in the regulation of skeletal differentiation^{74–76} and are involved in osteospecific differentiation via targeting of RUNX2.⁷⁷ To gain further insight into the molecular mechanisms underlying BMP2-induced osteogenic differentiation of hMSCs, we focused on miRNAs targeting RUNX2 and OSX. A search for miRNAs that were predicted to target RUNX2 and OSX was performed using the targetscan database and the extent of sequence conservation was examined using University of California Santa Cruz genome browser. The search results showed miR-23a and -23b are highly conserved and complementary to RUNX2 3'UTR

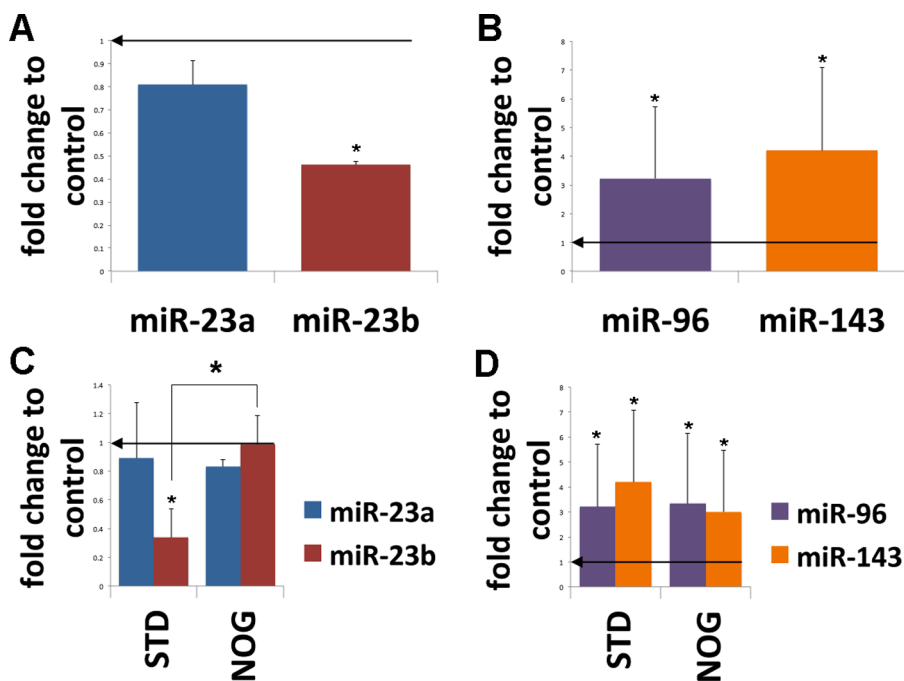


Figure 6. MicroRNA (miR) targeting of osteogenic transcription factors RUNX2 and OSX. (A) The expression of MiR-23a and -23b was assessed by qPCR after 5 days of MSC culture on NSQ50 at which time RUNX2 expression was maximal compared to on planar control. The data shows the expression of MiR-23a was unchanged and MiR-23b was down-regulated on NSQ50 suggesting negative regulation of RUNX2 by MiR-23b. (B) The expression of miRs-96 and -143 were measured after 9 days of MSC culture on NSQ50, at which time OSX expression was maximal compared to planar control. The data shows both miRs-96 and -143 were up-regulated suggesting positive regulation of OSX. (C) Expression of MiR-23a and -23b was assessed for MSCs cultured on NSQ50 and treated with the BMP signal inhibitor noggin compared to cells in standard culture. The data shows up-regulation of MiR-23b indicating MiR-23b is BMP2 dependent. (D) Expression of miRs-96 and -143 was unaffected by noggin suggesting BMP2 independence. All MiR qPCR data were normalized to the endogenous control small nuclear RNA U6. For qPCR data = mean \pm SD for $n = 3$ independent experiments (3 material replicated per experiment), *ANOVA $p < 0.05$. Arrows on graphs show the control level. NOG = noggin, STD = standard culture media.

(untranslated region), and miR-96 and -143 to the 3'UTR of OSX (Supporting Information, Figure S4).

Using qPCR, miR-23a and -23b were measured at day 5, and miR-96 and -143 at day 11 of culture on NSQ50 vs planar control, as RUNX2 and OSX were highly induced by the NSQ50 topography at day 5 and day 11 respectively. miR-23b was down-regulated in cells cultured on the nanotopography under normal culture conditions as compared with the planar control, while the abundance of miR-23a remained unchanged (Figure 6A). This indicates that miR-23b contributes to the activation of RUNX2 in hMSCs on NSQ50. In addition, when cells were exposed to noggin, the expression of miR-23b returned to the basal levels observed in cells cultured on the planar control (Figure 6C). This suggests that miR-23b targeting for RUNX2 was regulated by the BMP2 signal in cells on NSQ50. However, miR-96 and miR-143, which target the 3'UTR of OSX, were up-regulated in cells on the topography compared to the controls (Figure 6B) while overexpression of OSX was observed. Addition of noggin had no effect (Figure 6D) This suggests that the expression of miR-96 and -143 were independent of BMP2 signals. The activated expression of miR-96 and -143 correlated with the activated expression of OSX, suggesting that miR-96 and -143 most likely

had a positive regulatory role on OSX that was BMP-independent (perhaps through having a negative effect on OSX regulatory mRNAs). Together with the observations that the expression levels of Msx2 and Dlx5 were unchanged prior to the maximal increase in RUNX2 expression, this suggests that on the NSQ50 surface, BMP2-induced expression of RUNX2 is sufficient for OSX expression, and thus OSX expression is indirectly rather than directly linked to BMP signaling.

SUMMARY

There have been a number of reports of the roles of integrins and cytoskeletal tension on the osteospecific differentiation of hMCS. In this study, our osteoinductive NSQ50 topography was utilized to investigate the role of BMP2 in initiating osteogenic signaling in concert with cues from the integrins. We illustrate a role for BMP2 in the induction of RUNX2 through the repression of miR-23b. Subsequently, this induction of RUNX2 expression induced the transcription of OSX. These transcription factors then permitted the normal progression toward osteoblastic differentiation in line with classical guides.

It is notable that in hMCS on NSQ50, higher levels of the BMP receptor BMPR1a were observed at the transcript and protein level compared to planar controls,

apparently aiding the clustering of the integrin $\beta 5$ subunits that are used by hMSCs to adhere to vitronectin.

It is further noteworthy that very high levels of OPN, above levels of OCN, were expressed by the hMSCs on NSQ50. This may be related to the dual role of OPN as a protein containing the pro-adhesive tripeptide motif -RGD, as well as a calcium sequestering component of the ECM.

The temporal study indicates that hMSCs on planar control do not catch up with the osteospecific differentiation observed in cells on NSQ50 as levels of BMP, BMPR1a, RUNX2, OSX and ALP do not increase above NSQ50 levels as hMSCs on NSQ50 stop expressing

these markers. Thus, we show that cells on NSQ50 produce more osteoblasts rather than simply producing osteoblasts first (note that osteoblasts on the NSQ50 surface do go onto form mineral, Supporting Information, Figure S5).

This report further illustrates the potential for nanoscale materials in dissecting stem cell mechanisms without recourse to the use of soluble factors to drive differentiation. It also illustrates that osteogenesis on the NSQ50 material is a highly regulated process that appears to start with increased BMP2 sensitivity and then enter a well-orchestrated cascade of growth, transcriptional and extracellular matrix-modulating events.

MATERIALS AND METHODS

NSQ50 Nanotopography. A “near square” arrangement of nanopits with 120 nm diameter, 100 nm depth and with an average 300 nm center-to-center spacing with up to ± 50 nm offset were fabricated by electron beam lithography⁸ and replicated into $1 \times 1 \text{ cm}^2$ polycaprolactone (PCL) (cut from sheets of the polymer ϵ -polycaprolactone) by embossing on a hot plate at 70 °C as has been previously described.^{7,8}

Vitronectin (VN) Immobilization. NSQ50 surfaces were incubated with basal medium containing 5 $\mu\text{g}/\text{mL}$ of vitronectin at 4 °C for 24 h. The surface (NSQ50+NV) was washed with 1×PBS and prewarmed at 37 °C before MSCs were seeded on.

MSC Isolation and Culture. hMSCs were isolated from human bone marrow obtained from patients undergoing routine arthroplasty, with local ethical approval. Bone marrow aspirates were diluted 1:2 with basal medium (DMEM plus 10% FBS, 1% sodium pyruvate, 1% nonessential amino acids and 2% penicillin). Following cell separation on a Ficoll gradient, mononucleated cells were collected at the interphase and seeded into 75 cm^2 flask. After 3 days, fresh medium was added. Medium was changed every 3 days, and cells were subcultured at a 1:3 split using trypsin versine. Cells of passage 1 or 2 were used for experimental work. For seeding on to the biomaterial substrates cells were seeded with density of $1 \times 10^4 \text{ cells}/\text{cm}^2$. Cells were cultured in basal culture medium for the different time points used.

Cell Starvation. Cells were cultured in low serum medium, which contains DMEM, 1% FBS, 1% sodium pyruvate, 1% non essential amino acids and 2% penicillin, for 3 days, and then the low serum medium was replaced by fresh basal medium for the rest of the culture period.

BMP2 Antagonist Treatment. Human noggin protein (Sigma, UK) was dissolved in double processed tissue culture H₂O to a final concentration of 5 ng/ μL . Cells were seeded on PCL sheets in basal medium, and after allowing cells to settle down on the substrates, 10 μL noggin solution was added on to produce a final concentration 50 ng/mL. Cells were cultured in the presence of noggin for 5 days, then the medium was replaced with fresh medium without noggin (denoted as “blocked” in this report) for the rest of the culture period.

Quantitative Real-Time PCR (qRT-PCR). Cells were harvested, and total RNA was extracted using the RNeasy Micro kit (Invitrogen, UK). The total RNA was then reverse transcribed to cDNA using Superscript II reverse transcription kit (Invitrogen, UK). For microRNA, reverse transcription was performed using the Thermotranscript kit (Invitrogen, UK). The qRT-PCR was performed using a real time 7500 PCR machine (Applied Biosystems, UK) using the relative standard curve method. GAPDH served as endogenous control for protein encoding genes, and small nuclear RNA U6 for microRNA.

qRT-PCR Data Analysis. All data were normalized to endogenous control genes and planar control samples, and given

as mean \pm SD from three independent experiments. Statistical analysis was carried out using two-tailed ANOVAs for paired samples, and the threshold for statistical significance was set at a value of $p < 0.05$.

Immunofluorescence Staining. Cells were washed with 1×PBS and fixed with 10% formaldehyde solution at 37 °C for 15 min. Cells were then permeabilised using a buffer (10.3 g of NaCl, 0.06 g of MgCl₂H₂O, 0.476 g of HEPES in 100 mL of PBS, adjusted to pH 7.2 before adding 0.5 mL of Triton X) at 4 °C for 5 min. Cells were blocked for nonspecific binding using 1% BSA and incubating at 37 °C for 5 min. After blocking, the primary antibodies (Anti-RUNX2, cat. 05–1478, Millipore UK; Anti-OPN, sc-21742, Santa cruz biotechnology; Anti-BMPR1a, cat. 315-BR, R&D system; Anti-integrin $\beta 5$, cat. 4708, Cell signaling technology) against the proteins of interest along with phalloidin-rhodamine (Invitrogen, UK) were added and incubated at 37 °C for 1 h. Cells were next washed with 0.5% Tween in PBS (PBST) three times (5 min each). Then a biotinylated secondary antibody (Vector laboratories, UK) was added and incubated at 37 °C for 1 h followed by 3 × 5% PBST washing. Streptavidin-FITC (Vector Laboratories, UK) was added and incubated at 4 °C for 30 min followed by a 3 × 5% PBST wash. For nuclear visualization, a small drop of vectroshield-DAPI (Vector Laboratories, UK) was added before placing on the coverslip prior to fluorescence microscopy.

Immunoprecipitation. Proteins were isolated using lysis buffer and then centrifuged at 13 000 rpm for 15 min at 4 °C. The supernatant was transferred to a fresh tube with protein A agarose beads (Cat. 9863, Cell signaling technology) to preclean the samples. After 1 h of incubation at 4 °C, samples were centrifuged and collected into new tubes. Protein A agarose beads were incubated with primary antibodies (Human Integrin $\alpha v \beta 5$ antibody, cat. MAB2528, R&D systems) at 4 °C for 1 h and centrifuged at 4 °C for 2 min and the supernatant discarded. The mixture of primary antibody and agarose beads were washed with lysis buffer and then centrifuged, this was repeated three times. Equal amount of protein samples were added into mixture of primary antibody and agarose beads and incubated under rotation at 4 °C overnight. Samples were subsequently washed four times with lysis buffer and then proteins were eluted with SDS buffer for Western blot analysis.

Western Blot. Total protein was extracted from cells using RIPA lysis buffer. The lysate was collected and clarified by centrifugation at 13000 rpm for 5 min and supernatant transferred into a new tube. Protein was quantified using Quick Start Bradford protein assay Kit (Cat. 500–0203, BIO_RAD, UK). Total protein with concentration of 10 $\mu\text{g}/\text{mL}$ for each sample along with protein molecular weight marker heated at 95 °C for 5 min and then were loaded on 12-well 4–12% Bis-Tris-HCl polyacrylamide gels and run in 1×NuPAGE MOPS SDS running buffer at 200 V for 50 min. Proteins separated on the SDS-PAGE gel were transferred on to Hybond-N+ membrane (Amersham Bioscience, UK). The membrane was dried and then dipped in

methanol for 30 s, and then blocked in blocking buffer (1 g of nonfat dry milk in 20 mL of PBST) overnight at 4 °C. The blocked membrane was washed three times (10 min for each) with PBST buffer and then the membrane was incubated with primary antibody (Anti-RUNX2, cat. 05–1478, Millipore UK; Human BMP2 antibody, cat. MAB3551, R&D systems; Human Integrin $\alpha v\beta 5$ antibody, cat. MAB2528, R&D systems; Anti-BMPRI α , cat. 315-BR, R&D system; Anti-GAPDH, cat. ABS16, Millipore, UK) against the proteins (diluted 1:1000 in blocking buffer) at room temperature for 2 h followed by three washes (each for 10 min) with PBST buffer. The membrane was then incubated with secondary antibody (antimouse IgG-HRP, sc-2031; antirabbit IgG-HRP, sc-2030; antigen IgG-HRP, sc-2020; Santa Cruz technology) linked to a horseradish peroxidase (dilution 1:10 000 or 1:15 000 in blocking buffer) reporter enzyme at room temperature for 1 h followed by three washes (each for 10 min) with PBST buffer. The dried membrane was then immersed in colorimetric immunodetection reagents (Amersham Bioscience, UK) for 30 s and then dried on a soft tissue for X-ray viewing.

Metabolomics. Metabolite extraction from cells cultured on topographies and control samples for 1 week was done using ice cold chloroform:methanol:water (1:3:1, v/v) on a shaker for 1 h maintained at 4 °C. Samples were centrifuged, and 10 μ L of the supernatant injected on to the LC–MS system.

The LC separation was carried out using hydrophilic interaction chromatography with a ZIC-pHILIC 150 mm \times 4.6 mm, 5 μ m column (Merck Sequant), operated by an UltiMate liquid chromatography system (Dionex, Camberley, Surrey). The LC mobile phase was run with 20 mM ammonium carbonate in water (A) and acetonitrile (B). The mobile phase was run at a linear gradient for 15 min from 20–80% A, maintained at 5% A for 5 min and then re-equilibrated to 20% A. Mass spectrometric detection was performed using an Orbitrap Exactive (Thermo Fisher Scientific, Hemel Hempstead, U.K.) within the mass range *m/z* 70–1400 in polarity switching mode.

Chromatographic peak selection and metabolite identification were done using XCMS/Ideom/MzMatch analysis pipeline^{79,80} and measured peak intensities by LC–MS were normalized against protein content as measured using the Bradford assay as detailed previously.⁸¹ Metabolite identification were matched against a set of known standards within accurate mass (<3 ppm) and chromatographic retention time (<5%) windows. Compounds lacking metabolite standards were annotated using accurate mass and predicted retention time as described by Creek *et al.*⁸² All known metabolites associated with Kegg accession identifiers (KEGG ID#) were submitted to the KEGG database (http://www.genome.jp/kegg/tool/map_pathway1.html), and potentially relevant pathways were noted.

Conflict of Interest: The authors declare no competing financial interest.

Acknowledgment. J.Y. was supported by an EPSRC scholarship and most of the work was supported by BBSRC Grant BB/G008868/1. M.J.D., R.M.D.M. and N.G. are supported by grants from BBSRC, MRC and EPSRC.

Supporting Information Available: Metabolic pathways and targetscan sequences. This material is available free of charge via the Internet at <http://pubs.acs.org>.

REFERENCES AND NOTES

- Benoit, D. S.; Durney, A. R.; Anseth, K. S. The Effect of Heparin-Functionalized Peg Hydrogels on Three-Dimensional Human Mesenchymal Stem Cell Osteogenic Differentiation. *Biomaterials* **2007**, *28*, 66–77.
- Calve, S.; Odelberg, S. J.; Simon, H. G. A Transitional Extracellular Matrix Instructs Cell Behavior During Muscle Regeneration. *Dev. Biol.* **2010**, *344*, 259–271.
- Carey, S. P.; Kranning-Rush, C. M.; Williams, R. M.; Reinhart-King, C. A. Biophysical Control of Invasive Tumor Cell Behavior by Extracellular Matrix Microarchitecture. *Biomaterials* **2012**, *33*, 4157–4165.
- Yang, L. M.; Liu, Y.; Zhao, J.; Hao, L. M.; Huang, K. X.; Jiang, W. H. Characterization of Human Umbilical Cord Mesenchymal Stem Cells Following Tissue Mass Culture. *Cell Mol. Biol.* **2014**, *60*, 12–18.
- Choi, B. H.; Choi, Y. S.; Kang, D. G.; Kim, B. J.; Song, Y. H.; Cha, H. J. Cell Behavior on Extracellular Matrix Mimic Materials Based on Mussel Adhesive Protein Fused with Functional Peptides. *Biomaterials* **2010**, *31*, 8980–8988.
- Choi, C. H.; Hagvall, S. H.; Wu, B. M.; Dunn, J. C.; Beygui, R. E.; CJ, C. J. K. Cell Interaction with Three-Dimensional Sharp-Tip Nanotopography. *Biomaterials* **2007**, *28*, 1672–1679.
- Chung, N.; Jee, B. K.; Chae, S. W.; Jeon, Y. W.; Lee, K. H.; Rha, H. K. Hox Gene Analysis of Endothelial Cell Differentiation in Human Bone Marrow-Derived Mesenchymal Stem Cells. *Mol. Biol. Rep.* **2009**, *36*, 227–235.
- Dalby, M. J.; Gadegaard, N.; Tare, R.; Andar, A.; Riehle, M. O.; Herzyk, P.; Wilkinson, C. D.; Oreffo, R. O. The Control of Human Mesenchymal Cell Differentiation Using Nanoscale Symmetry and Disorder. *Nat. Mater.* **2007**, *6*, 997–1003.
- Dalby, M. J.; Riehle, M. O.; Johnstone, H.; Affrossman, S.; Curtis, A. S. In Vitro Reaction of Endothelial Cells to Polymer Demixed Nanotopography. *Biomaterials* **2002**, *23*, 2945–2954.
- Price, R. L.; Haberstroh, K. M.; Webster, T. J. Enhanced Functions of Osteoblasts on Nanostructured Surfaces of Carbon and Alumina. *Med. Biol. Eng. Comput.* **2003**, *41*, 372–375.
- Dalby, M. J.; Riehle, M. O.; Johnstone, H. J.; Affrossman, S.; Curtis, A. S. Polymer-Demixed Nanotopography: Control of Fibroblast Spreading and Proliferation. *Tissue Eng.* **2002**, *8*, 1099–1108.
- Yim, E. K. F.; Reano, R. M.; Pang, S. W.; Yee, A. F.; Chen, C. S.; Leong, K. W. Nanopattern-Induced Changes in Morphology and Motility of Smooth Muscle Cells. *Biomaterials* **2005**, *26*, 5405–5413.
- McMurray, R. J.; Gadegaard, N.; Tsimbouri, P. M.; Burgess, K. V.; McNamara, L. E.; Tare, R.; Murawski, K.; Kingham, E.; Oreffo, R. O.; Dalby, M. J. Nanoscale Surfaces for the Long-Term Maintenance of Mesenchymal Stem Cell Phenotype and Multipotency. *Nat. Mater.* **2011**, *10*, 637–644.
- Tsimbouri, P. M.; McMurray, R. J.; Burgess, K. V.; Alakpa, E. V.; Reynolds, P. M.; Murawski, K.; Kingham, E.; Oreffo, R. O.; Gadegaard, N.; Dalby, M. J. Using Nanotopography and Metabolomics to Identify Biochemical Effectors of Multipotency. *ACS Nano* **2012**, *6*, 10239–10249.
- Zouani, O. F.; Chanseau, C.; Brouillaud, B.; Bareille, R.; Deliane, F.; Foulc, M. P.; Mehdi, A.; Durrieu, M. C. Altered Nanofeature Size Dictates Stem Cell Differentiation. *J. Cell Sci.* **2012**, *125*, 1217–1224.
- Das, R. K.; Zouani, O. F.; Labrugere, C.; Oda, R.; Durrieu, M. C. Influence of Nanohelical Shape and Periodicity on Stem Cell Fate. *ACS Nano* **2013**, *7*, 3351–3361.
- Yim, E. K.; Darling, E. M.; Kulangara, K.; Guilak, F.; Leong, K. W. Nanotopography-Induced Changes in Focal Adhesions, Cytoskeletal Organization, and Mechanical Properties of Human Mesenchymal Stem Cells. *Biomaterials* **2010**, *31*, 1299–1306.
- Chen, W.; Villa-Diaz, L. G.; Sun, Y.; Weng, S.; Kim, J. K.; Lam, R. H.; Han, L.; Fan, R.; Krebsbach, P. H.; Fu, J. Nanotopography Influences Adhesion, Spreading, and Self-Renewal of Human Embryonic Stem Cells. *ACS Nano* **2012**, *6*, 4094–4103.
- Kingham, E.; White, K.; Gadegaard, N.; Dalby, M. J.; Oreffo, R. O. Nanotopographical Cues Augment Mesenchymal Differentiation of Human Embryonic Stem Cells. *Small* **2013**, *9*, 2140–2151.
- Kingham, E.; Oreffo, R. O. Embryonic and Induced Pluripotent Stem Cells: Understanding, Creating, and Exploiting the Nano-Niche for Regenerative Medicine. *ACS Nano* **2013**, *7*, 1867–1881.
- Ji, L.; LaPointe, V. L.; Evans, N. D.; Stevens, M. M. Changes in Embryonic Stem Cell Colony Morphology and Early Differentiation Markers Driven by Colloidal Crystal Topographical Cues. *Eur. Cell Mater.* **2012**, *23*, 135–146.

22. Bianco, P.; Riminucci, M.; Gronthos, S.; Robey, P. G. Bone Marrow Stromal Stem Cells: Nature, Biology, and Potential Applications. *Stem Cells* **2001**, *19*, 180–192.
23. Yang, X.; Tare, R. S.; Partridge, K. A.; Roach, H. I.; Clarke, N. M.; Howdle, S. M.; Shakesheff, K. M.; Oreffo, R. O. Induction of Human Osteoprogenitor Chemotaxis, Proliferation, Differentiation, and Bone Formation by Osteoblast Stimulating Factor-1/Pleiotrophin: Osteoconductive Biomimetic Scaffolds for Tissue Engineering. *J. Bone Miner. Res.* **2003**, *18*, 47–57.
24. Bianco, P.; Cao, X.; Frenette, P. S.; Mao, J. J.; Robey, P. G.; Simmons, P. J.; Wang, C. Y. The Meaning, the Sense and the Significance: Translating the Science of Mesenchymal Stem Cells into Medicine. *Nat. Med.* **2013**, *19*, 35–42.
25. Mirmalek-Sani, S. H.; Tare, R. S.; Morgan, S. M.; Roach, H. I.; Wilson, D. I.; Hanley, N. A.; Oreffo, R. O. Characterization and Multipotentiality of Human Fetal Femur-Derived Cells: Implications for Skeletal Tissue Regeneration. *Stem Cells* **2006**, *24*, 1042–1053.
26. Wen, J. H.; Vincent, L. G.; Fuhrmann, A.; Choi, Y. S.; Hribar, K. C.; Taylor-Weiner, H.; Chen, S.; Engler, A. J. Interplay of Matrix Stiffness and Protein Tethering in Stem Cell Differentiation. *Nat. Mater.* **2014**, *10*.1038/nmat4051.
27. Murphy, W. L.; McDevitt, T. C.; Engler, A. J. Materials as Stem Cell Regulators. *Nat. Mater.* **2014**, *13*, 547–557.
28. Engler, A. J.; Sen, S.; Sweeney, H. L.; Discher, D. E. Matrix Elasticity Directs Stem Cell Lineage Specification. *Cell* **2006**, *126*, 677–689.
29. Benoit, D. S.; Schwartz, M. P.; Durney, A. R.; Anseth, K. S. Small Functional Groups for Controlled Differentiation of Hydrogel-Encapsulated Human Mesenchymal Stem Cells. *Nat. Mater.* **2008**, *7*, 816–823.
30. Curran, J. M.; Stokes, R.; Irvine, E.; Graham, D.; Amro, N. A.; Sanedrin, R. G.; Jamil, H.; Hunt, J. A. Introducing Dip Pen Nanolithography as a Tool for Controlling Stem Cell Behaviour: Unlocking the Potential of the Next Generation of Smart Materials in Regenerative Medicine. *Lab Chip* **2010**, *10*, 1662–1670.
31. Dalby, M. J.; Gadegaard, N.; Oreffo, R. O. Harnessing Nanotopography and Integrin-Matrix Interactions to Influence Stem Cell Fate. *Nat. Mater.* **2014**, *13*, 558–569.
32. Oh, S.; Brammer, K. S.; Li, Y. S.; Teng, D.; Engler, A. J.; Chien, S.; Jin, S. Stem Cell Fate Dictated Solely by Altered Nanotube Dimension. *Proc. Natl. Acad. Sci. U. S. A.* **2009**, *106*, 2130–2135.
33. Park, J.; Bauer, S.; Schlegel, K. A.; Neukam, F. W.; von der Mark, K.; Schmuki, P. TiO₂ Nanotube Surfaces: 15 nm—An Optimal Length Scale of Surface Topography for Cell Adhesion and Differentiation. *Small* **2009**, *5*, 666–671.
34. Park, J.; Bauer, S.; von der Mark, K.; Schmuki, P. Nanosize and Vitality: TiO₂ Nanotube Diameter Directs Cell Fate. *Nano Lett.* **2007**, *7*, 1686–1691.
35. Sjostrom, T.; McNamara, L. E.; Meek, R. M.; Dalby, M. J.; Su, B. 2d and 3d Nanopatterning of Titanium for Enhancing Osteoinduction of Stem Cells at Implant Surfaces. *Adv. Healthcare Mater.* **2013**, *2*, 1285–1293.
36. McNamara, L. E.; Sjostrom, T.; Burgess, K. E.; Kim, J. J.; Liu, E.; Gordonov, S.; Moghe, P. V.; Meek, R. M.; Oreffo, R. O.; Su, B.; Dalby, M. J. Skeletal Stem Cell Physiology on Functionally Distinct Titania Nanotopographies. *Biomaterials* **2011**, *32*, 7403–7410.
37. Vieu, C.; Carcenac, F.; Pepin, A.; Chen, Y.; Mejias, M.; Lebib, A.; Manin-Ferlazzo, L.; Couraud, L.; Launois, H. Electron Beam Lithography: Resolution Limits and Applications. *Appl. Surf. Sci.* **2000**, *164*, 111–117.
38. Kwan, A. P.; Cummings, C. E.; Chapman, J. A.; Grant, M. E. Macromolecular Organization of Chicken Type X Collagen *In Vitro*. *J. Cell Biol.* **1991**, *114*, 597–604.
39. Tsimbouri, P. M.; McMurray, R. J.; Burgess, K. V.; Alakpa, E. V.; Murawski, K.; Kingham, E.; Oreffo, R. O. C.; Gadegaard, N.; Dalby, M. J. A Using Nanotopography and Metabolomics to Identify Biochemical Effectors of Multipotency. *ACS Nano* **2012**, *6*, 10239–10249.
40. Dalby, M. J.; Gadegaard, N.; Oreffo, R. O. Harnessing Nanotopography and Integrin-Matrix Interactions to Influence Stem Cell Fate. *Nat. Mater.* **2014**, *13*, 558–569.
41. Dalby, M. J.; Gadegaard, N.; Tare, R.; Andar, A.; Riehle, M. O.; Herzyk, P.; Wilkinson, C. D.; Oreffo, R. O. The Control of Human Mesenchymal Cell Differentiation Using Nano-scale Symmetry and Disorder. *Nat. Mater.* **2007**, *6*, 997–1003.
42. Arnold, M.; Cavalcanti-Adam, E. A.; Glass, R.; Blummel, J.; Eck, W.; Kantlehner, M.; Kessler, H.; Spatz, J. P. Activation of Integrin Function by Nanopatterned Adhesive Interfaces. *ChemPhysChem* **2004**, *5*, 383–388.
43. Cavalcanti-Adam, E. A.; Volberg, T.; Micoulet, A.; Kessler, H.; Geiger, B.; Spatz, J. P. Cell Spreading and Focal Adhesion Dynamics Are Regulated by Spacing of Integrin Ligands. *Biophys. J.* **2007**, *92*, 2964–2974.
44. Schvartzman, M.; Palma, M.; Sable, J.; Abramson, J.; Hu, X.; Sheetz, M. P.; Wind, S. J. Nanolithographic Control of the Spatial Organization of Cellular Adhesion Receptors at the Single-Molecule Level. *Nano Lett.* **2011**, *11*, 1306–1312.
45. Ingber, D. E. Cellular Mechanotransduction: Putting All the Pieces Together Again. *FASEB J.* **2006**, *20*, 811–827.
46. Biggs, M. J.; Richards, R. G.; Gadegaard, N.; Wilkinson, C. D.; Dalby, M. J. The Effects of Nanoscale Pits on Primary Human Osteoblast Adhesion Formation and Cellular Spreading. *J. Mater. Sci.: Mater. Med.* **2007**, *18*, 399–404.
47. Kilian, K. A.; Bugarija, B.; Lahn, B. T.; Mrksich, M. Geometric Cues for Directing the Differentiation of Mesenchymal Stem Cells. *Proc. Natl. Acad. Sci. U. S. A.* **2010**, *107*, 4872–4877.
48. Zhao, M.; Harris, S. E.; Horn, D.; Geng, Z.; Nishimura, R.; Mundy, G. R.; Chen, D. Bone Morphogenetic Protein Receptor Signaling Is Necessary for Normal Murine Postnatal Bone Formation. *J. Cell Biol.* **2002**, *157*, 1049–1060.
49. Afzal, F.; Pratap, J.; Ito, K.; Ito, Y.; Stein, J. L.; van Wijnen, A. J.; Stein, G. S.; Lian, J. B.; Javed, A. Smad Function and Intracellular Targeting Share a Runx2Motif Required for Osteogenic Lineage Induction and Bmp2 Responsive Transcription. *J. Cell Physiol.* **2005**, *204*, 63–72.
50. Massague, J.; Seoane, J.; Wotton, D. Smad Transcription Factors. *Genes Dev.* **2005**, *19*, 2783–2810.
51. Shi, Y.; Massague, J. Mechanisms of Tgf-Beta Signaling from Cell Membrane to the Nucleus. *Cell* **2003**, *113*, 685–700.
52. Guicheux, J.; Lemonnier, J.; Ghayor, C.; Suzuki, A.; Palmer, G.; Caverzasio, J. Activation of P38 Mitogen-Activated Protein Kinase and C-Jun-Nh2-Terminal Kinase by Bmp-2 and Their Implication in the Stimulation of Osteoblastic Cell Differentiation. *J. Bone Miner. Res.* **2003**, *18*, 2060–2068.
53. Lai, C. F.; Cheng, S. L. Alphavbeta Integrins Play an Essential Role in Bmp-2 Induction of Osteoblast Differentiation. *J. Bone Miner. Res.* **2005**, *20*, 330–340.
54. Stein, G. S.; Lian, J. B. Molecular Mechanisms Mediating Proliferation/Differentiation Interrelationships During Progressive Development of the Osteoblast Phenotype. *Endocr. Rev.* **1993**, *14*, 424–442.
55. Deng, Z. L.; Sharff, K. A.; Tang, N.; Song, W. X.; Luo, J.; Luo, X.; Chen, J.; Bennett, E.; Reid, R.; Manning, D.; Xue, A.; Montag, A. G.; Luu, H. H.; Haydon, R. C.; He, T. C. Regulation of Osteogenic Differentiation During Skeletal Development. *Front. Biosci.* **2008**, *13*, 2001–2021.
56. Duxy, P.; Zhang, R.; Geoffroy, V.; Ridall, A. L.; Karsenty, G. Osf2/Cbfα1: A Transcriptional Activator of Osteoblast Differentiation. *Cell* **1997**, *89*, 747–754.
57. Hassan, M. Q.; Tare, R. S.; Lee, S. H.; Mandeville, M.; Morasso, M. I.; Javed, A.; van Wijnen, A. J.; Stein, J. L.; Stein, G. S.; Lian, J. B. Bmp2 Commitment to the Osteogenic Lineage Involves Activation of Runx2 by Dlx3 and a Homeodomain Transcriptional Network. *J. Biol. Chem.* **2006**, *281*, 40515–40526.
58. Hassan, M. Q.; Javed, A.; Morasso, M. I.; Karlin, J.; Montecino, M.; van Wijnen, A. J.; Stein, G. S.; Stein, J. L.; Lian, J. B. Dlx3 Transcriptional Regulation of Osteoblast Differentiation: Temporal Recruitment of Msx2, Dlx3, and Dlx5 Homeodomain Proteins to Chromatin of the Osteocalcin Gene. *Mol. Cell. Biol.* **2004**, *24*, 9248–9261.
59. Kim, Y. J.; Kim, H. N.; Park, E. K.; Lee, B. H.; Ryoo, H. M.; Kim, S. Y.; Kim, I. S.; Stein, J. L.; Lian, J. B.; Stein, G. S.;

- van Wijnen, A. J.; Choi, J. Y. The Bone-Related Zn Finger Transcription Factor Osterix Promotes Proliferation of Mesenchymal Cells. *Gene* **2006**, *366*, 145–151.
60. Nishio, Y.; Dong, Y.; Paris, M.; O'Keefe, R. J.; Schwarz, E. M.; Drissi, H. Runx2-Mediated Regulation of the Zinc Finger Osterix/Sp7 Gene. *Gene* **2006**, *372*, 62–70.
61. Liu, W.; Toyosawa, S.; Furuchi, T.; Kanatani, N.; Yoshida, C.; Liu, Y.; Himeno, M.; Narai, S.; Yamaguchi, A.; Komori, T. Overexpression of Cbfa1 in Osteoblasts Inhibits Osteoblast Maturation and Causes Osteopenia with Multiple Fractures. *J. Cell Biol.* **2001**, *155*, 157–166.
62. Geoffroy, V.; Kneissel, M.; Fournier, B.; Boyde, A.; Matthias, P. High Bone Resorption in Adult Aging Transgenic Mice Overexpressing Cbfa1/Runx2 in Cells of the Osteoblastic Lineage. *Mol. Cell. Biol.* **2002**, *22*, 6222–6233.
63. Sabri, A.; Ziaeef, A. A.; Ostad, S. N.; Alimoghadam, K.; Ghahremani, M. H. Crosstalk of Egf-Directed Mapk Signaling Pathways and Its Potential Role on Egf-Induced Cell Proliferation and Cox-2 Expression in Human Mesenchymal Stem Cells. *Cell Biochem. Funct.* **2011**, *29*, 64–70.
64. Zayzafoon, M. Calcium/Calmodulin Signaling Controls Osteoblast Growth and Differentiation. *J. Cell. Biochem.* **2006**, *97*, 56–70.
65. Chang, S. C.-N.; Chuang, H.; Chen, Y.-R.; Yang, L.-C.; Chen, J.-K.; Mardini, S.; Chung, H.-Y.; Lu, Y.-L.; Ma, W.-C.; Lou, J.; Mardinis, S. Cranial Repair Using Bmp-2 Gene Engineered Bone Marrow Stromal Cells. *J. Surg. Res.* **2004**, *119*, 85–91.
66. Shibuya, H.; Yamaguchi, K.; Shirakabe, K.; Tonegawa, A.; Gotoh, Y.; Ueno, N.; Irie, K.; Nishida, E.; Matsumoto, K. Tab1: An Activator of the Tak1Mapkk in Tgf-Beta Signal Transduction. *Science* **1996**, *272*, 1179–1182.
67. Hynes, R. O.; Lively, J. C.; McCarty, J. H.; Taverna, D.; Francis, S. E.; Hodivala-Dilke, K.; Xiao, Q. The Diverse Roles of Integrins and Their Ligands in Angiogenesis. *Cold Spring Harbor Symp. Quant. Biol.* **2002**, *67*, 143–153.
68. Huvemeers, S.; Danen, E. H. Adhesion Signaling—Crosstalk between Integrins, Src and Rho. *J. Cell Sci.* **2009**, *122*, 1059–1069.
69. Ivaska, J.; Heino, J. Interplay between Cell Adhesion and Growth Factor Receptors: From the Plasma Membrane to the Endosomes. *Cell Tissue Res.* **2010**, *339*, 111–120.
70. Biggs, M. J.; Richards, R. G.; McFarlane, S.; Wilkinson, C. D.; Oreffo, R. O.; Dalby, M. J. Adhesion Formation of Primary Human Osteoblasts and the Functional Response of Mesenchymal Stem Cells to 330nm Deep Microgrooves. *J. R. Soc., Interface* **2008**, *5*, 1231–1242.
71. Biggs, M. J.; Richards, R. G.; Gadegaard, N.; Wilkinson, C. D.; Oreffo, R. O.; Dalby, M. J. The Use of Nanoscale Topography to Modulate the Dynamics of Adhesion Formation in Primary Osteoblasts and Erk/Mapk Signalling in Stro-1+ Enriched Skeletal Stem Cells. *Biomaterials* **2009**, *30*, 5094–5103.
72. McBeath, R.; Pirone, D. M.; Nelson, C. M.; Bhadriraju, K.; Chen, C. S. Cell Shape, Cytoskeletal Tension, and Rhoa Regulate Stem Cell Lineage Commitment. *Dev. Cell* **2004**, *6*, 483–495.
73. Malmstrom, J.; Lovmand, J.; Kristensen, S.; Sundh, M.; Duch, M.; Sutherland, D. S. Focal Complex Maturation and Bridging on 200 nm Vitronectin but Not Fibronectin Patches Reveal Different Mechanisms of Focal Adhesion Formation. *Nano Lett.* **2011**, *11*, 2264–2271.
74. Chen, J. F.; Mandel, E. M.; Thomson, J. M.; Wu, Q.; Callis, T. E.; Hammond, S. M.; Conlon, F. L.; Wang, D. Z. The Role of MicroRNA-1 and MicroRNA-133 in Skeletal Muscle Proliferation and Differentiation. *Nat. Genet.* **2006**, *38*, 228–233.
75. Mizuno, Y.; Tokuzawa, Y.; Ninomiya, Y.; Yagi, K.; Yatsuka-Kanesaki, Y.; Suda, T.; Fukuda, T.; Katagiri, T.; Kondoh, Y.; Amemiya, T.; Tashiro, H.; Okazaki, Y. Mir-210 Promotes Osteoblastic Differentiation through Inhibition of Acvr1b. *FEBS Lett.* **2009**, *583*, 2263–2268.
76. Mizuno, Y.; Yagi, K.; Tokuzawa, Y.; Kanesaki-Yatsuka, Y.; Suda, T.; Katagiri, T.; Fukuda, T.; Maruyama, M.; Okuda, A.; Amemiya, T.; Kondoh, Y.; Tashiro, H.; Okazaki, Y. Mir-125b Inhibits Osteoblastic Differentiation by Down-Regulation of Cell Proliferation. *Biochem. Biophys. Res. Commun.* **2008**, *368*, 267–272.
77. Huang, J.; Zhao, L.; Xing, L.; Chen, D. MicroRNA-204 Regulates Runx2 Protein Expression and Mesenchymal Progenitor Cell Differentiation. *Stem Cells* **2010**, *28*, 357–364.
78. Gadegaard, N.; Thoms, S.; MacIntyre, D. S.; McGhee, K.; Gallagher, J.; Casey, B.; Wilkinson, C. D. W. Arrays of Nano-Dots for Cellular Engineering. *Microelectron. Eng.* **2003**, *67–68*, 162–168.
79. Creek, D. J.; Jankevics, A.; Burgess, K. E. V.; Breitling, R.; Barrett, M. P. Ideom: An Excel Interface for Analysis of LC–MS Based Metabolomics Data. *Bioinformatics* **2012**, *28*, 1048–1049.
80. Scheltema, R. A.; Jankevics, A.; Jansen, R. C.; Swertz, M. A.; Breitling, R. Peakml/Mzmatch: A File Format, Java Library, R Library, and Tool-Chain for Mass Spectrometry Data Analysis. *Anal. Chem.* **2011**, *83*, 2786–2793.
81. Compton, S. J.; Jones, C. G. Mechanism of Dye Response and Interference in the Bradford Protein Assay. *Anal. Biochem.* **1985**, *151*, 369–374.
82. Creek, D. J.; Jankevics, A.; Breitling, R.; Watson, D. G.; Barrett, M. P.; Burgess, K. E. V. Toward Global Metabolomics Analysis with Hydrophilic Interaction Liquid Chromatography–Mass Spectrometry: Improved Metabolite Identification by Retention Time Prediction. *Anal. Chem.* **2011**, *83*, 8703–8710.